# Evaluating the Potential of High Spatial Resolution Spaceborne InSAR for Monitoring Ground Deformation Hazards in Challenging Mountainous Terrains

Farnoush Hosseini, Bernhard Rabus, Manuele Pichierri
*Simon Fraser University, Burnaby, BC, Canada*
Marc-André Brideau
*BGC Engineering Inc., Vancouver, BC, Canada*

ABSTRACT
In this study we investigate the potential of high-resolution Synthetic Aperture Radar Interferometry (InSAR) to gain added insight into monitoring landslides with difficult characteristics such as steep terrain, strong spatially heterogeneous motion, and coherence-compromising factors such as vegetation and seasonal snow cover. Using TerraSAR-X (TSX) Staring Spotlight data, we demonstrate novel analysis methods specifically tailored to high-resolution data for two sites in British Columbia; the Hope Slide scarp, and the summit area of Mount Currie. The data include 22 TerraSAR-X images acquired in staring spotlight mode from 2015 to 2017 from a descending orbit for the Hope scarp, and 12 images from June to September 2017 from both ascending and descending orbits for the Mount Currie site. High-resolution Digital Elevation Models (DEM) of the two areas are generated from LiDAR observations, to accurately remove the topographic and atmospheric effects from the interferograms. The resulting displacement residuals reveal new movement hotspots and unprecedented spatial detail for active landslides and rock falls at the investigated sites.

RÉSUMÉ
Dans ce projet nous étudions le potentiel de donnée radar interférométrique à ouverture synthétique (InSAR) à très haute résolution pour avoir une meilleure compréhension de la surveillance de glissements de terrain avec des caractères compliqués comme terrain très escarpé, des déplacements inhomogènes, et des facteurs qui réduise la cohérence tel que la végétation et la neige saisonnière. En utilisant les données TerraSAR-X (TSX) Staring Spotlight, nous démontrons une nouvelle méthode d'analyse spécifique au donnée haute résolution pour deux sites en Colombie-Britannique, La zone de départ du glissement de Hope et le sommet du Mont Currie. Les données incluent 22 images TerraSAR-X acquises en mode Staring Spotlight de 2015 à 2017 en orbite descendant pour l'escarpement de glissement de Hope, et 12 images de juin à septembre 2017 d'orbite ascendant et descendant pour le Mont Currie. Les modèles numériques de terrain (MNT) des deux régions sont obtenus de donnée de télédétection par laser, pour pouvoir enlever de façon rigoureuse les effets topographique et atmosphérique de l'intérférograme Les déplacements résiduels révèle de nouvelles zones de mouvements en détails et résolution sans précédent pour les zone de chute de pierres et glissement au deux cas d'études.

## 1 INTRODUCTION

Landslides pose serious threats to human life and infrastructure including buildings, mines, and transportation networks. Human and financial losses due to landslide disasters occur worldwide. At the same time, landslides are potentially among the most manageable natural hazards, provided a deeper understanding of their mechanisms is available. Long-term consistent monitoring of landslides is key to uncovering threats and the drivers and mechanisms of the ground movement. Assessing slope stability by means of state-of-the-art ground based and remote sensing techniques provides timely, high quality information on landslide precursor motion that is spatially comprehensive and representative. Satellite remote sensing is particularly useful for steep and rugged topography that renders representative in-situ ground monitoring expensive and challenging. Combining temporally dense high resolution monitoring from space with initial in situ geological assessments ultimately holds the best promise to help stakeholders reduce the human and economic impact of future landslide events.

### 1.1 InSAR

Synthetic Aperture Radar Interferometry (InSAR) is a powerful tool for monitoring displacements of the Earth surface and of man-made structures on this surface, given InSAR's ability to generate dense and accurate deformation maps over spans of days to years in nearly-all weather conditions (Hooper 2008). Such maps are obtained by exploiting the phase difference between two complex valued SAR images, acquired from different orbit positions and/or at different times (Lauknes 2004).
TSX is ideal for monitoring landslides given its ability to capture displacements on the scale of the short X band wavelength (3 cm) with wide coverage, and short revisit time (11 days). By providing very high spatial resolution (< 50 cm) SAR data, the novel TSX Staring Spotlight mode is the most suitable option to meet the criteria of detecting subtle and small-scale movements in rugged terrain. Such terrain can exhibit a large number of disjointed surface facets separated by lay-over and shadow regions. The enhancement of existing InSAR processing techniques to make full use of the synergistic combination of high spatial resolution SAR imagery and LiDAR is expected to improve

significantly the inverted deformation measurements for challenging landslide prone slopes.

## 1.2 Case Studies

The stability of two representative sites in British Columbia, the Hope Slide scarp, and Mount Currie's summit area are investigated with TSX Staring Spotlight observations. We explain the reasons for choosing these areas and their special characteristics in the next two subsections.

### 1.2.1 Hope Slide

The Hope Slide (Figure 1) was one of the largest landslides recorded in Canada. It occurred in January 1965, in the Nicolum Valley in the Cascade Mountains near the municipality of Hope, British Columbia (Donati et al. 2017). The landslide buried Highway 3 under 47 million cubic metres of rock (Mathews and McTaggart 1978).

By using SAR remote sensing, we intend to perform a comprehensive analysis of slope stability on and around Hope Slide to better understand the triggers and dynamics of mass movements in the area.

Brideau et al. (2005) recognized seven faults and three dominantly brittle shear zones in the Hope Slide area. Tension cracks and trench-like features have also been recorded adjacent to the slide scar (Von Sacken 1991). The aforementioned tectonic features are shown in Figure 2.

To evaluate the influence of these tectonic structures on the rock mass damage, the Geological Strength Index (GSI) of the rocks at 72 stations over the Hope Slide was measured (Brideau et al. 2005). The lowest GSI values (Figure 3) were recorded along the northwestern headscarp, where the tectonic features including shear zones and faults are located. This significant correlation between these features and the derived GSI values suggests that the Hope slide was caused by the present tectonic structures (Brideau et al. 2005).

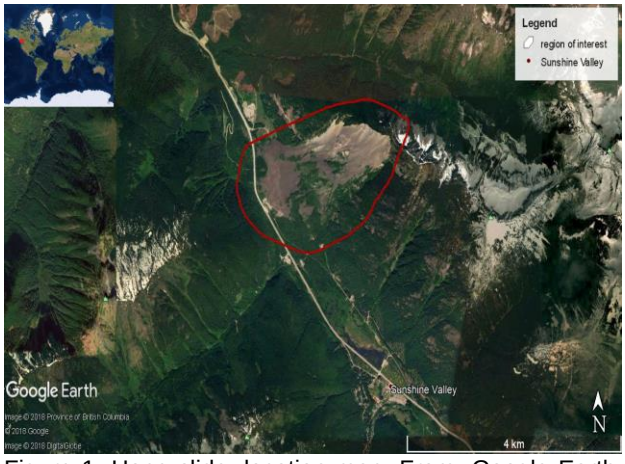


Figure 1. Hope slide: location map. From: Google Earth, December 2016. The red polygon highlights the region of interest.

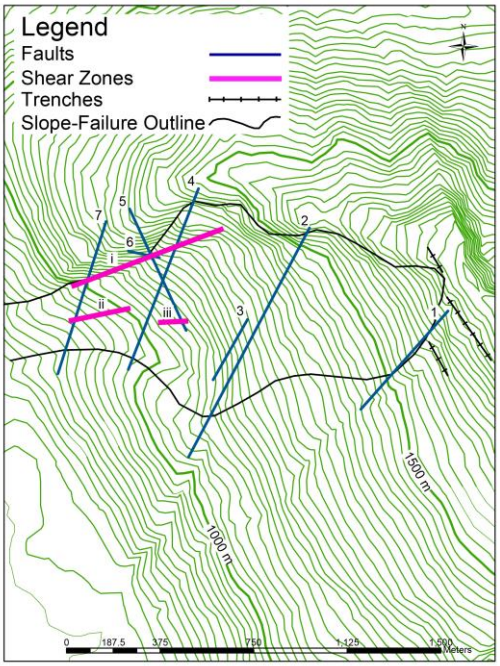


Figure 2. Hope Slide: Location of the faults, shear zones, and trenches. (From: Brideau et al. 2005)

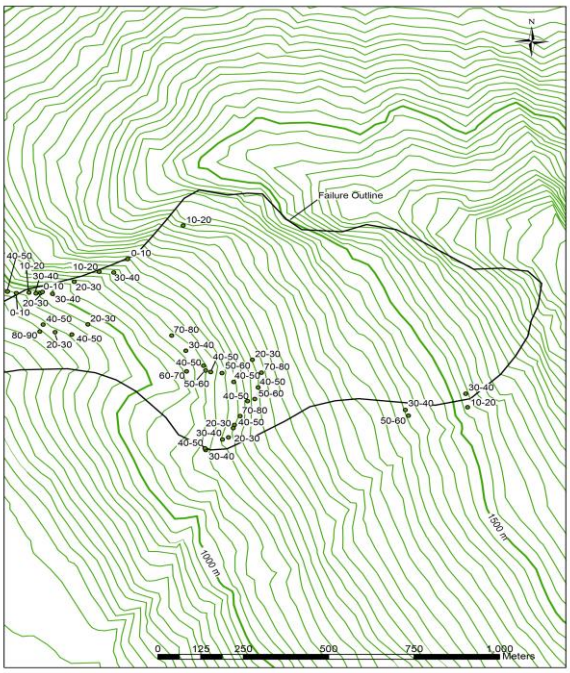


Figure 3. GSI estimates for the greenstone unit at the Hope Slide (From: Brideau et al. 2005)

### 1.2.2 Mount Currie

Mount Currie is the summit peak of a northeast trending ridge above the village of Pemberton and Hamlet of Mount Currie, BC (Figure 4). A series of rock fall events occurred near the ridge crest in 2015 and 2016. The rock fall

activities, which may be pre-cursors to a more catastrophic event associated with tectonic structures close to the Mount Currie ridge line, raised concerns about the safety of human lives and infrastructures in the nearby communities.

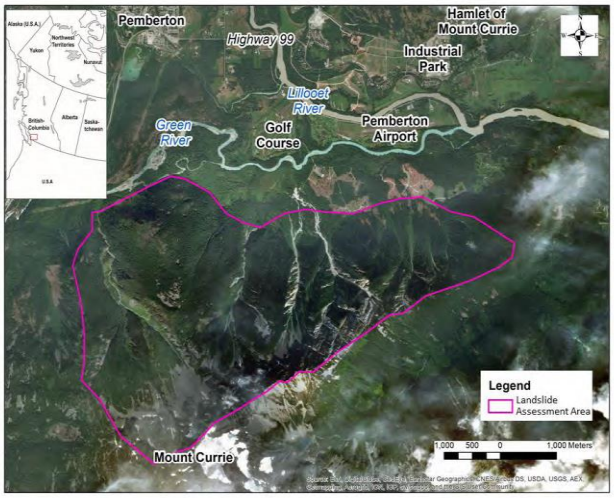


Figure 4. Mount Currie: location map, August 2014, From (BGC Enginnering 2018). The purple polygon highlights the region of interest.

To investigate the probability of a massive rock avalanche it is crucial to detect the deformation features of the area. Mount Currie's deformation features as plausible sources for rock avalanche scenarios are listed as follows:

- Three sets of lineaments, which foreshadow slope failures, were found on Mount Currie. One set of lineaments, source ID 2, includes the main tension cracks along the ridgeline. A second set of lineaments, source ID 1, corresponds to numerous scars and may be associated with tension cracks on the west side of Mount Currie. The third set of lineaments, Source ID 5 and 6, corresponds to the orientation of gullies and persistent traces on the steep rock slope of the north face of Mount Currie (BGC Enginnering 2018).
- Deep-Seated Gravitational Slope Deformation (DSGSD) related features, including uphill facing scarps, ridge top trenches and grabens, or scarps with talus were identified at multiple locations within Mount Currie. The potential rock avalanche source zones with IDs 1, 2, 3, 4, 13 and 15 in Figure 6 are representative of this deformation feature (BGC Enginnering 2018).
- Rock falls are commonplace on Mount Currie and often form talus slope with limited runout distance at the base of rock slopes. Zones 10 and 11 represent the current rock falls occurred in 2015 and 2016 respectively. Tension cracks along and near Mount Currie ridge may trigger rock falls and cause instability (source IDs 7 and 12). Rock slides have also been recorded at several locations on Mount Currie (source ID 16) (BGC Enginnering 2018).

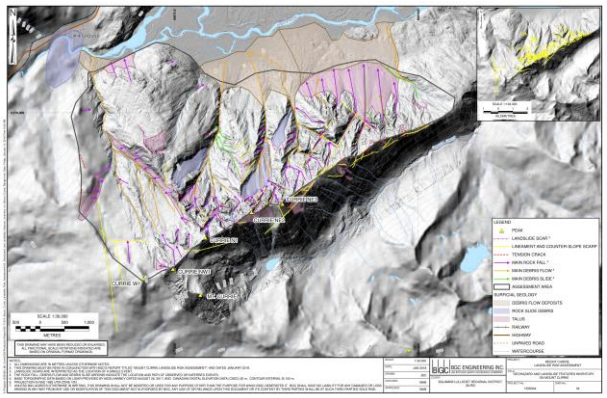

Figure 5. Mount Currie: Geohazard and landslide features. From: (BGC Enginnering 2018)

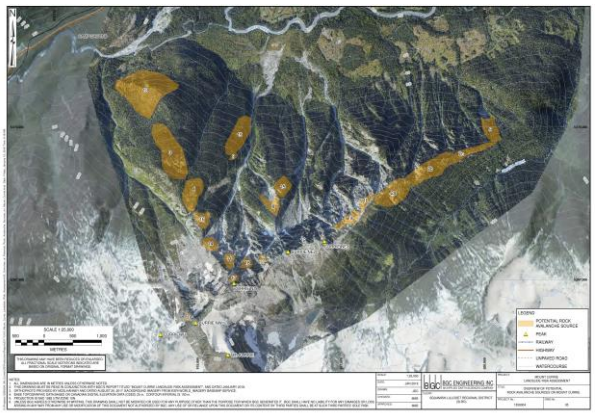

Figure 6. Mount Currie: Overview of potential rock avalanche sources. From: (BGC Enginnering 2018)

## 2 METHODS

The TSX data are processed to obtain accurate surface displacement maps. For each site all data is first co-registered to a common master geometry to form the interferometric image stack. Pairwise interferograms (I) can then be formed from any two co-registered images $y_1$ and $y_2$ using appropriate common band filtering and complex conjugate multiplication (Rosen et al. 2000).

$$I = y_1 y_2^* = |y_1||y_2|\exp(\mathrm{j}(\phi_1 - \phi_2)) \quad [1]$$

The phase of each interferogram, $\phi_{\mathrm{int}} = \phi_1 - \phi_2$, can be parameterized as (Hanssen 2001):

$$\phi_{\mathrm{int}} = \phi_{def} + \phi_{\mathrm{topo}} + \phi_{atm} + \phi_{ref} + \phi_n \quad [2]$$

In equation [2]:

- The deformation term $\Phi_{\mathrm{def}}$ accounts for (temporal) changes in phase occurring between the two acquisitions, e.g. owing to surface movement or dielectric changes.
- The term $\Phi_{\mathrm{topo}}$ arises when the two acquisitions are acquired from slightly different satellite positions and is sensitive to surface topography.

- $\Phi_{atm}$ is the phase equivalent to the propagation delays due to atmospheric water vapor variations in time and space. This quantity can be modelled as the sum of a "static" atmospheric term, which is a function of elevation, and a "dynamic" atmospheric term (based on the dynamic nature of the troposphere).
- The reference phase or "flat earth" phase $\Phi_{ref}$ is caused by effect of the earth's curvature on the phase.
- The term $\Phi_n$ accounts for any residual phase noise.

For high spatial resolution data the deformation term $\Phi_{def}$ is estimated from equation [2] by appropriately modeling/estimating and compensating the other phase terms as follows:

- $\Phi_{topo}$ is estimated using a high-resolution DEM of the area.
- $\Phi_{ref}$ is derived from the accurate satellite orbital information by measuring the distance between satellite and the Earth reference ellipsoid for each resolution cell in the image.
- The static atmospheric term in $\Phi_{atm}$ is estimated as a function of ground elevation via the iterative algorithm detailed in Figure 7. In each iteration, slope and offset of the trend between phase and elevation are estimated using a least squares fitting technique over an area where phase variation is within 2π (the size of this area increases with the iterations). It should be noted that all the pixels with suspected surface deformation have been masked out prior to carrying out the fit.
- The dynamic atmospheric phase in $\Phi_{atm}$ is estimated via a uniform filter with a large sliding window corresponding to about 4 km on the ground applied over the interferogram. Again, all areas of suspected movement have been masked out prior to applying this low-pass filter (Rabus and Ghuman 2009). Note that the interferograms corrected in this way might still be affected by a residual atmospheric phase, which will usually be small except for one or both images capturing a more extreme weather event such as a strong storm or cold front event. For each case study, all the interferograms have been also scrutinized manually to identify presence of excessive remnant atmospheric-related phase patterns in the SAR acquisitions. Interferograms formed from acquisitions with the least residual atmospheric patterns can then be selected.

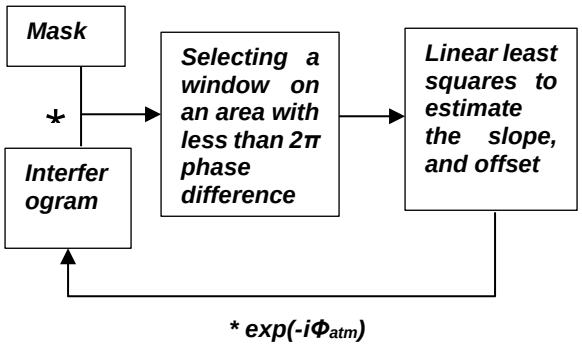


Figure 7. Static atmospheric phase removal: Flowchart of the adopted iterative method.

## 3 DATA

The SAR dataset consists of 22 Staring Spotlight TSX images from a descending orbit between 2015 and 2017 for the Hope Slide scarp site, and 4 ascending along with 8 descending orbit Staring Spotlight TSX images for the Mount Currie site from June to September 2017. The outline of the SAR frames used is shown in Figure 8.

To remove the topographic and atmospheric effects from interferometric observations, we generated high-resolution Digital Elevation Models (DEMs) of the investigated areas by blending the high resolution (1m) LiDAR, with the low resolution SRTM (30m). For this, we used a thin-plate spline fit that minimizes distortions and stitching errors during the blending procedure. The generated DEMs are displayed in Figure 9.

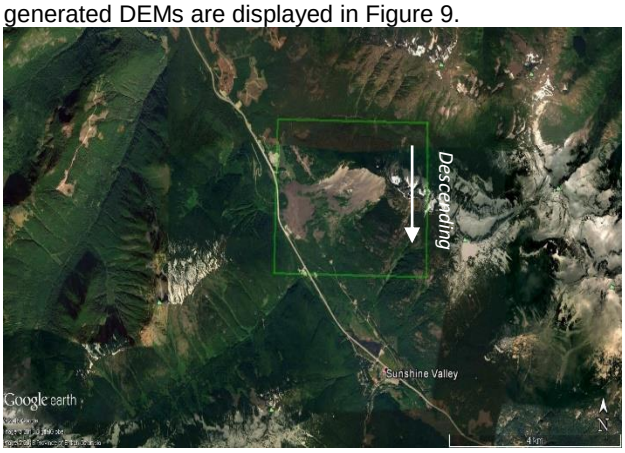


(a)


(b)

Figure 8. TSX footprints (in green) for (a) Hope Slide (b) Mount Currie. From: Google Earth.

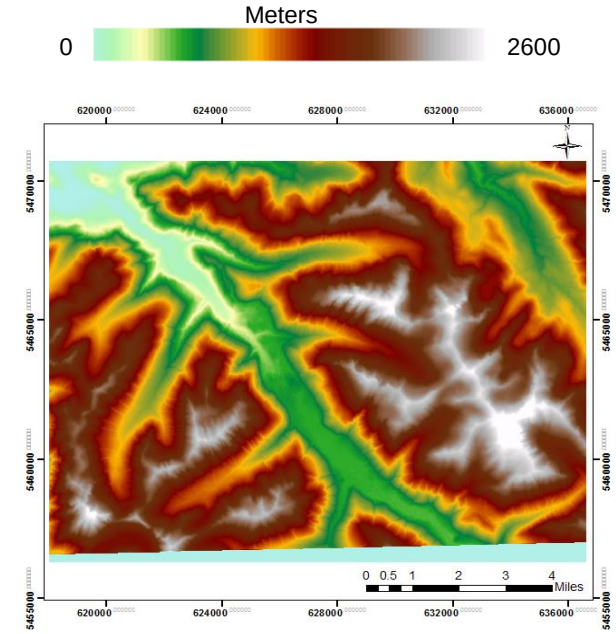


(a)

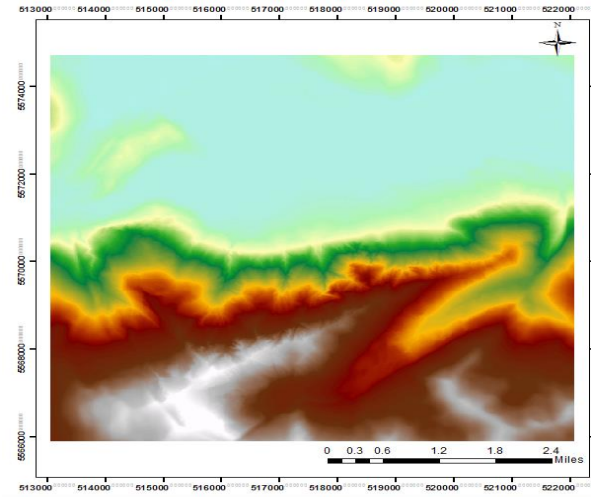


(b)

Figure 9. Generated DEMs for (a) Hope Slide (b) Mount Currie case study sites.

## 4 RESULTS

### 4.1 Hope Slide

Figure 10 shows an interferogram with a small spatial baseline of 160 meters; spanning August 2015 to September 2017, that is close to the maximum observed time period. Four areas of observed deformation are highlighted in red.

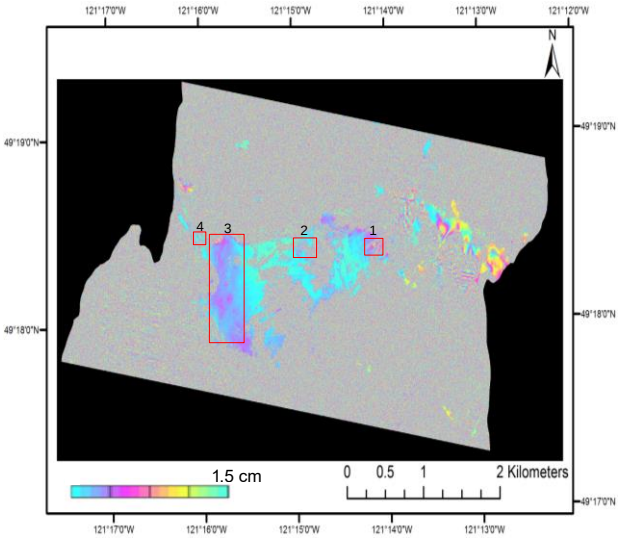


Figure 10. Hope Slide: Geocoded TSX interferogram (15 Aug 2015 - 23 Sep 2017). The four areas where deformation is observed are highlighted in red.

The first area identifies a new area with rock fall potential near the headscarp of the Hope Slide. The most evident deformation feature is a small region containing a full interferometric color fringe indicative of a strong deformation gradient. The field photographs acquired by BGC Engineering Inc. suggest clear evidence of instability in this area (Figure 11).

The second area is located in another active part of the landslide in terms of rock falls (Figure 12). This area is located near faults and a shear zone (see Figure 2), where the rock mass exhibits low GSI values according to Figure 3. The concentration of the regional tectonic features that leads to the reduced rock-mass quality can cause onset of rock falls or slides compatible with the deformation pattern observed in the interferogram. Another photograph (Figure 12) corroborates the possibility of rock falls and slides for this second area.

The third area shows subtle movement in the accumulation zone of the Hope Slide, where the debris of the historic landslide has accumulated and created a bulge (Figure 13). In this region, the interferogram suggests subtle movement away from the SAR sensor and along the line-of-sight (LOS) direction. This may indicate secondary slides in the deposits of the historic landslide, or alternatively subsidence/ settling of the bulge.

Figure 11. Hope Slide: Field photograph of area no. 1 in Figure 10

Figure 12. Hope Slide: Field photograph of the northwestern side of the slide

Figure 13. Hope Slide: Field photograph of the accumulation zone.

The fourth area is a small deforming patch located near Highway 3. This area corresponds to the distal edge of the coarse portion of the 1965 Hope Slide deposit (see Figure 14). As the movement is captured in the LOS direction, there are two possible deformation scenarios: either the landslide deposit might be subject to subsidence on its eastern side, or the eastern side of the hill is experiencing a slow landslide. Although the deformation is subtle in this zone, at its current rate it may lead to minor damage to the road prism and a need for maintenance.


Figure 14: Hope Slide: Deforming area near Highway 3 (red polygon) corresponding to distal limit of coarse debris From: Google Earth.

4.2 Mount Currie

Figure 15 shows a suitable interferogram over the period July and September 2017. Besides having a negligible identified residual atmospheric phase for both acquistions of the pair, this interferogram also has the smallest spatial baseline (5m) and longest possible temporal baseline from our data record to date. The interferogram is computed using descending orbit acquisitions, as the focus of the study is on the northern face of Mount Currie. Owing to the rugged topography of the area and the steep incidence angle (ca. 22 degrees), this face is completely in layover for ascending orbit interferograms, which makes it impossible to retrieve deformation in that geometry.
As shown in the figure, surface movements are observed in two areas on the northern face of Mount Currie (highlighted in red).

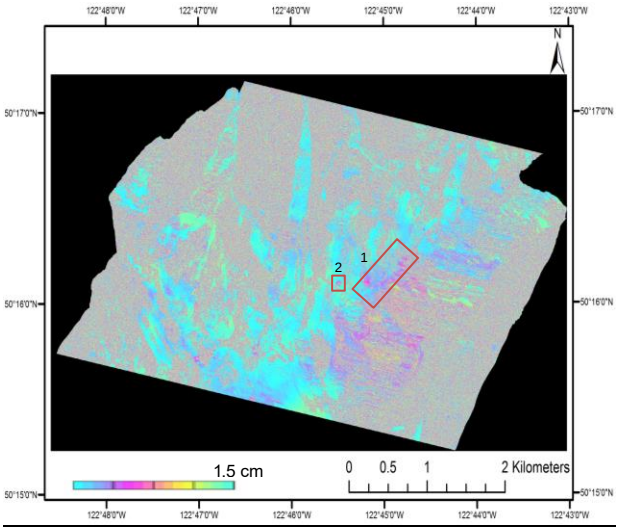


Figure 15. Mount Currie: Geocoded TSX interferogram (2 Jul 2017 - 6 Sep 2017). The two areas where deformation is observed are highlighted in red.

The first region, which is situated along the ridge east of Currie NE3 Peak, is a source for potential rock avalanches according to the BGC report (area 2a and 2b in Figure 6). The interferogram indicates ongoing deformation (potentially toppling) in this area, which encompasses the main tension cracks (Figure 16). The deformation observed in the interferogram is consistent with the scenario described elsewhere (BGC Enginnering 2018) and also compatible with the deformation pattern previously documented in this area (Bovis and Evans 1995). According to this scenario, a rock avalanche event in this area might dam Green and Lillooet rivers, damage the airport, and affectt the Golf course.

The second area shows another noticeable block movement occurring near a zone characterized by a deep-seated gravitational slope deformation delimited by tension cracks (source ID 1a, see Figure 6). Figure 17 shows the disturbed shape of rocks in this area, which suggests the potential of rock falls.

Figure 16. Mount Currie: Field photograph of a disturbed rock mass in area no. 1 of Figure 15. From: BGC Engineering 2018).

Figure 17. Mount Currie: Field photograph of a disturbed rock mass in area no. 2 of Figure 15 (from: BGC Engineering report).

## 5 CONCLUSION

We used very high resolution spaceborne InSAR data (TSX Staring Spotlight) to carry out stability analyses of two sites in BC; the area of the Hope Slide and the summit ridge of Mount Currie. High resolution DEMs of both areas were generated from LIDAR observations for the InSAR processing. The high coherence and unprecedented spatial detail of the results indicate excellent suitability of TSX Staring Spotlight data for identification and monitoring of small-scale landslides in challenging mountainous areas.

The observed movements in LOS direction of the satellite revealed that both sites, especially Mount Currie, are susceptible to future rock falls at small scales. Our results highlight the need for a larger stack of interferometric measurements allowing rigorous time series analyses to gain a deeper understanding of the movement mechanisms. Continued assessment of the sites with high resolution InSAR over longer time periods is expected to quantify the likelihood of larger events; rock avalanches or landslides, a help avoid future losses.

## 6 ACKNOWLEDGMENT

We would like to thank German Aerospace Agency (DLR) for acquiring and providing TerraSAR-X images under the proposals LAN3540_rabus and LAN2465_rabus, respectively. This work has been performed in collaboration with BGC Engineering Inc. in the framework of the NSERC Engage project “Integrated processing of high-resolution spaceborne InSAR and LiDAR to produce better displacement map series for landslides”.

## 7 REFERENCES

BGC Enginnering, I. 2018. MOUNT CURRIE LANDSLIDE RISK ASSESSMENT.

Bovis, M.J., and Evans, S.G. 1995. Rock slope movements along the Mount Currie" fault scarp," southern Coast Mountains, British Columbia. Canadian Journal of Earth Sciences **32**(12): 2015-2020.

Brideau, M.-A., Stead, D., Kinakin, D., and Fecova, K. 2005. Influence of tectonic structures on the Hope Slide,

British Columbia, Canada. Engineering geology **80**(3): 242-259.
Donati, D., Stead, D., Brideau, M., and Ghirotti, M. 2017. A remote sensing approach for the derivation of numerical modelling input data: insights from the Hope Slide, Canada. *In* ISRM AfriRock - Rock Mechanics for Africa. Internation Society for Rock Mechanics and and Rocke Engineering, Cape Town, South Africa.
Hanssen, R.F. 2001. Radar interferometry: data interpretation and error analysis. *In* Radar interferometry. *Edited by* F.V.d. Meer. Springer Science & Business Media.
Hooper, A. 2008. A multi-temporal InSAR method incorporating both persistent scatterer and small baseline approaches. Geophysical Research Letters **35**(16).
Lauknes, T.R. 2004. Long-term surface deformation mapping using small-baseline differential SAR interferograms. Unpublished Master Thesis, Department of Physics and Technology, University of Tromso, Norway.
Mathews, W., and McTaggart, K. 1978. Hope rockslides, British Columbia, Canada. *In* Developments in Geotechnical Engineering. Elsevier. pp. 259-275.
Rabus, B.T., and Ghuman, P.S. 2009. A simple robust two-scale phase component inversion scheme for persistent scatterer interferometry (dual-scale PSI). Can. J. Remote Sens. **35**(4): 399-410.
Rosen, P.A., Hensley, S., Joughin, I.R., Li, F.K., Madsen, S.N., Rodriguez, E., and Goldstein, R.M. 2000. Synthetic aperture radar interferometry. Proceedings of the IEEE **88**(3): 333-382.
Von Sacken, R.S. 1991. New data and re-evaluation of the 1965 Hope Slide, British Columbia. University of British Columbia.